Registry No. **3a**, 76174-09-9; **3b**, 55498-97-0; **4a**, 76174-10-2; **4b**, 63148-50-5; SbF_3, 7783-56-4; **5**, 76174-11-3; **6**, 76174-12-4.

Supplementary Material Available: Compilations of observed and calculated structure factor amplitudes for **4a** and **4b**, thermal parameters (Table VII), refined hydrogen atom coordinates (Table VIII), and bond lengths and angles for phenyl groups and those involving hydrogen atoms (Table IX) for **4a**, and similar data for **4b** (Tables IX–XI) (24 pages). Ordering information is given on any current masthead page.

Contribution No. 6219 from the Department of Chemistry, California Institute of Technology, Pasadena, California 91125, and the School of Chemical Sciences, University of Illinois, Urbana, Illinois 61801

Binuclear Complexes of Macrocyclic Ligands: Variation of Magnetic Exchange Interaction in a Series of Six-Coordinate Iron(II), Cobalt(II), and Nickel(II) Complexes and the X-ray Structure of a Binuclear Iron(II) Macrocyclic Ligand Complex

CLIFFORD L. SPIRO,[1] SUSAN L. LAMBERT,[2] THOMAS J. SMITH,[1] EILEEN N. DUESLER,[2] ROBERT R. GAGNÉ,*[1] and DAVID N. HENDRICKSON*[2]

Received July 30, 1980

The X-ray crystal and molecular structure of $[LFe_2(Im)_4](BF_4)_2$, where Im is imidazole and L is the dianion of the binucleating ligand 11,23-dimethyl-3,7,15,19-tetraazatricyclo[19.3.1.1^{9,13}]hexacosa-2,7,9,11,13(26),14,19,21(25),22,24-decaene-25,26-diol, has been determined on a Syntex $P2_1$ diffractometer. A total of 2468 reflections at the $1.5\sigma(I)$ significance level were used to give final discrepancy indices of $R_1 = 0.082$ and $R_2 = 0.083$. The complex crystallizes in the monoclinic space group $C2/c$ in a cell having the dimensions $a = 21.060$ (5) Å, $b = 17.138$ (4) Å, $c = 12.172$ (2) Å, and $\beta = 108.82$ (2)°. The observed and calculated densities are 1.53 and 1.52 g/cm^3, respectively. Four formula units comprise the unit cell with half of the binuclear complex in the asymmetric unit. Discrete $[LF_2(Im)_4]^{2+}$ cations and BF_4^- anions were found. The binuclear cations are centrosymmetric with each iron(II) ion being six-coordinate by virtue of interactions with two nitrogen and two oxygen atoms of the binucleating ligand L and two nitrogen atoms each from the imidazole ligands. The ligand L is planar except for the two trimethylene bridges. The two iron ions are only 0.011 (1) Å out of this ligand plane with an Fe–Fe distance of 3.117 (2) Å and Fe–N(imidazole) distances of 2.218 Å. Variable-temperature (4.2–286 K) magnetic susceptibility data are given for the binuclear high-spin six-coordinate complexes $[LNi_2(py)_4](BF_4)_2$, $[LCo_2(py)_4](BF_4)_2$, $[LFe_2(py)_4](BF_4)_2$, $[LFe_2(Im)_4](BF_4)_2$, $[LFe_2(MeIm)_4](BF_4)_2$, and $[LFe_2(MeNic)_4](BF_4)_2$, where py is pyridine, Im is imidazole, MeIm is 1-methylimidazole, and MeNic is the methyl ester of isonicotinic acid. in each case an antiferromagnetic exchange interaction is present. The data were least-squares fit to the susceptibility equations resultant from the Hamiltonian $\hat{H} = -2J\hat{S}_1\cdot\hat{S}_2$ to give exchange parameters (J) of −23 (Ni^{2+}), −4.1 (Co^{2+}) and −7.5 cm^{-1} (Fe^{2+}) for the three pyridine complexes. Values of $J = -6.8$, −4.5, and −1.5 cm^{-1} were obtained for the other three high-spin iron(II) complexes with MeNic, MeIm, and Im axial ligands, respectively. It was found that there is little difference in the magnitude of magnetic exchange interaction between LM_2Cl_2 (M = Fe(II), Co(II), and Ni(II)) with five-coordinate metal ions and the corresponding complex in the $[LM_2(py)_4](BF_4)_2$ series with six-coordinate metal ions. An increase in antiferromagntic exchange interaction was expected for a six-coordinate complex compared to the analogous five-coordinate complex as a consequence of improved orbital overlap from the metal ion being in the plane of the binucleating ligand for the six-coordinate complex. This was not realized, possibly because the increased ligand field splitting in the six-coordinate complex attenuated the increased antiferromagnetic interaction.

Introduction

Complexes of the binucleating ligand LH_2 can be formed

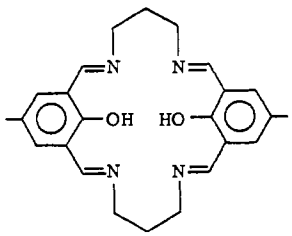

LH_2

from the condensation of 2 mol of 2,6-diformyl-4-methylphenol with 2 mol of 1,3-diaminopropane in the presence of divalent transition-metal ions.[3] X-ray structural work,[4,5] on $LCu_2Cl_2\cdot 6H_2O$ and $LCo_2Br_2\cdot CH_3OH$ has shown that the metal ion coordination geometry is square pyramidal with one halide ion bonded to each metal ion in an axial site. The cobalt(II) ion is further out of the L ligand plane (0.30 Å) than is the copper(II) ion (0.21 Å).

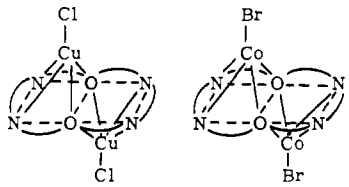

In a recent paper[6] we reported variable-temperature magnetic susceptibility data for a series of complexes of L including $LCu_2Cl_2\cdot 6H_2O$, $LNi_2Cl_2\cdot 2H_2O$, $LCo_2Br_2\cdot CH_3OH$, LMn_2Cl_2, and LFe_2Cl_2. The magnetic exchange interaction observed for each complex was assessed with the isotropic spin Ham-

(1) California Institute of Technology.
(2) University of Illinois.
(3) Pilkington, N. H.; Robson, R. *Aust. J. Chem.* **1970**, *23*, 2225.
(4) Hoskins, B. F.; Williams, G. A. *Aust. J. Chem.* **1975**, *28*, 2607.
(5) Hoskins, B. F.; McLeod, N. J.; Schaap, H. A. *Aust. J. Chem.* **1976**, *29*, 515.
(6) Lambert, S. L.; Hendrickson, D. N. *Inorg. Chem.* **1979**, *18*, 2683.

0020-1669/81/1320-1229$01.25/0

iltonian $\hat{H} = -2J\hat{S}_1\cdot\hat{S}_2$. A strong antiferromagnetic interaction is seen for the copper complex where $J = -294$ cm^{-1}. The net antiferromagnetic interaction decreases monotonically in the series copper, nickel ($J = -27$ cm^{-1}), cobalt ($J = -9.3$ cm^{-1}), and iron ($J = -4.2$ cm^{-1}), to finally become a net ferromagnetic exchange interaction in the manganese complex ($J = +0.2$ cm^{-1}). The variation in J value across this series was attributed to an increasing number of unpaired electrons and also to an increasing metal–ligand plane distance in going from copper(II) to manganese(II).

In this paper the preparation and physical properties of a series of binuclear complexes of ligand L with six-coordinate metal ions are reported. The new complexes are $[LNi_2(py)_4](BF_4)_2$, $[LCo_2(py)_4](BF_4)_2$, $[LFe_2(py)_4](BF_4)_2$, $[LFe_2(Im)_4](BF_4)_2$, $[LFe_2(MeIm)_4](BF_4)_2$ and $[LFe_2(MeNic)_4](BF_4)_2$, where py is pyridine, Im is imidazole, MeIm is 1-methylimidazole, and MeNic is the methyl ester of isonicotinic acid. The single-crystal X-ray structure of $[LFe_2(Im)_4](BF_4)_2$ is also reported. The point of enquiry of the present paper is whether the magnetic exchange interaction is responsive to a change in the metal ion coordination geometry from five-coordinate to six-coordinate.

Experimental Section

Compound Preparation. All reagents and solvents were purchased from commercial sources and used without further purification unless otherwise described. 2,6-Diformyl-4-methylphenol was prepared according to literature methods.[7] Ferrous tetrafluoroborate hexahydrate was prepared by heating iron filings with 50% fluoroboric acid under an inert atmosphere. *Caution*: rapid hydrogen evolution. The pale green solution was evaporated under vacuum, leaving pale blue crystals of $Fe(BF_4)_2\cdot 6H_2O$ which were removed by filtration, vacuum-dried, and stored under an inert atmosphere.

Binuclear Iron Complexes $LFe_2(base)_4(BF_4)_2$. Under an inert atmosphere 1,3-diaminopropane (1.0 mL) was added dropwise to a hot (50 °C) solution (30 mL) of base (base = pyridine, 1-methylimidazole, or methyl isonicotinate) containing ferrous tetrafluoroborate (1.8 g). A solution (20 mL) of hot base containing 2,6-diformyl-4-methylphenol (0.82 g) was added with stirring. Slow addition of an equal volume of distilled water afforded purple crystals of $LFe_2(Base)_4(BF_4)_2$. These were collected and stirred with petroleum ether (30–60 °C) overnight to remove excess base and were vacuum-dried. Where base = pyridine, slow evolution of pyridine from the solid resulted in continual weight loss. Anal. Calcd for $[LFe_2(MeIm)_4](BF_4)_2$, $C_{40}H_{50}N_{12}O_2Fe_2B_2F_8$: C, 45.00; H, 4.37; N, 17.50; Fe, 11.7. Found: C, 45.15; H, 4.50; N, 17.05; Fe, 12.0. Anal. Calcd for $[LFe_2(MeNic)_4](BF_4)_2$, $C_{52}H_{54}N_8O_{10}Fe_2B_2F_8$: C, 50.89; H, 4.40; N, 9.13. Found: C, 50.65; H, 4.30; N, 9.15. Anal. Calcd for $LFe_2(py)_{3.5}](BF_4)_2$, C, 51.60; H, 4.51; N, 10.90; Fe, 10.90. Found: C, 50.95; H, 4.8; N, 10.69; Fe, 10.8. Note loss of pyridine in analysis.

Preparation of $[LFe_2(Im)_4](BF_4)_2$. All manipulations leading to this compound were carried out either in a Vacuum Atmospheres glovebox or in a Schlenk apparatus under an atmosphere of argon gas. The methanol used was distilled under argon and stored over 4-Å molecular sieves. Ferrous tetrafluoroborate tetrahydrate (2.09 g) was dissolved in methanol (10 mL). Equimolar quantities of 1,3-diaminopropane and 2,6-diformyl-4-methylphenol, dissolved in minimum quantities of methanol, were added sequentially. The solution was refluxed 45 min before imidazole (2.29 g) in methanol (10 mL) was added, and the refluxing was continued for an additional 80 min. A small volume of solvent was removed, and the purple microcrystalline solid which formed was filtered off. Anal. Calcd: C, 45.03; H, 4.41; N, 17.51; Fe, 11.63. Found: C, 45.00; H, 4.35; N, 17.35; Fe, 11.3. The crystals used in the structure determination were grown from the filtrate of the above reaction on standing at ca. −10 °C for 2 weeks under argon. The analysis of the crystals is given. Anal. Calcd: C, 45.03; H, 4.41; N, 17.51; Fe, 11.63. Found: C, 45.00; H, 4.30; N, 18.05; Fe, 11.05.

Binuclear Co and Ni Complexes. The following procedure is typical of the methods used to prepare the binuclear cobalt and nickel complexes. Into a pyridine solution (20 mL) of 2,6-diformyl-4-methylphenol (0.20 g, 1.22 mmol), 1,3-diaminopropane (0.1 mL, 1.20 mmol) was pipetted with stirring and mild heating. Previously dried $Co(BF_4)_2\cdot 6H_2O$ (0.43 g, 1.85 mmol) in methanol (5 mL) was added to the pyridine solution which became deep red-brown. Heating was continued as the solution volume was reduced to a few milliliters while orange crystals formed. After the mixture was cooled, the precipitate was collected by filtration, washed with a small amount of pyridine followed by a larger quantity of diethyl ether, and vacuum-dried. Anal. Calcd for $C_{44}H_{46}N_8O_2B_2Co_2F_8$: C, 52.3; H, 4.6; N, 11.1. Found: C, 51.9; H, 4.6; N, 11.0.

Identical procedures afforded orange crystals of $[LCo_2(py)_4](ClO_4)_2$ and dull gold-brown microcrystalline samples of $[LNi_2(py)_4](BF_4)_2$ and $[LNi_2(py)_4](ClO_4)_2$. Anal. Calcd for $C_{44}H_{46}N_8O_{10}Cl_2Co_2$: C, 51.0; H, 4.5; N, 10.8. Found: C, 50.7; H, 4.5; N, 10.8. Calcd for $C_{44}H_{46}N_8O_2B_2F_8Ni_2$: C, 52.3; H, 4.6; N, 11.1. Found: C, 52.2; H, 4.7; N, 11.7. Calcd for $C_{44}H_{46}N_8O_{10}Cl_2Ni_2$: C, 51.0; H, 4.5; N, 10.8. Found: C, 51.1; H, 4.7; N, 10.8.

The cobalt compounds appear to be reactive, somewhat, toward oxygen in solution but not in the solid state. All the complexes are soluble in polar organic solvents, and loss of pyridine in the solids appears to be negligible.

Physical Measurements. Infrared spectra were recorded on a Beckman 4240 infrared spectrophotometer as Nujol mulls between NaCl plates. Electronic absorption spectra were obtained with a Cary 14 spectrophotometer with 1-cm quartz cells for solution studies and as mulls on filter paper for solids with the solvent in both cases in the reference compartment. Faraday magnetic susceptibility measurements were accomplished with use of a Cahn Instruments Faraday balance with powdered samples at room temperature with $HgCo(SCN)_4$ as a calibrant. Diamagnetic corrections were made by using Pascal's constants.

A PAR Model 150A vibrating-sample magnetometer operated at 13.5 kG, was used to obtain the magnetic susceptibility data at various temperatures down to 4.2 K. Data for various samples of $CuSO_4\cdot 5H_2O$ were periodically run in the range of 4.2–286 K and were used to standardize the system.[8] In addition, two samples of $[Ni(qnqn)Cl_2]_2$, where qnqn is *trans*-2-(2-quinolyl)methylene-3-quinuclidinone, were run at different times to ensure the data obtained previously for this same compound.[9] A calibrated GaAs diode was employed for determination of the sample temperature. A correction for the diamagnetism of the sample container and the background was made at all temperatures to the data for all compounds. The data were also corrected for the diamagnetism for each compound with estimated values from Pascal's constants.[10] The resulting molar paramagnetic susceptibilities were least-squares fit to the appropriate theoretical susceptibility expressions by means of a computer program.[11]

Table I. Experimental Data for the X-ray Diffraction Study of $[LFe_2(Im)_4](BF_4)_2$

Crystal Parameters	
$a = 21.060$ (5) Å	space group = $C2/c$
$b = 17.138$ (4) Å	$Z = 4$ (binuclear units)
$c = 12.172$ (2) Å	mol wt 956.09
$\beta = 108.82$ (2)°	ρ(calcd) = 1.52 g/cm^3
monoclinic	ρ(exptl) = 1.53 g/cm^3 (flotation in bromoform–methylene chloride)
	$V = 4158.3$ Å^3

Measurement of Intensity Data
radiatn: Mo Kα (λ 0.710 69 Å)
monochromator: graphite crystal
monochromator angle: 6.2°
X-ray beam collimator diameter: 1.0 mm
cryst orientation: random
reflctns measd: (h,k,l) and $(-h,-k,-l)$
max 2θ: 55°
scan type: θ–2θ scan technique
scan speed: 3–29.3°/min
base width: 2.25°
bkg measurement: bkg counting/total scan time = 0.5

(7) Ullmann, F.; Brittner, K. *Chim. Ber.* **1909**, *42*, 2539.

(8) Reekie, J. *Proc. R. Soc. London* **1939**, *173*, 367.

(9) Laskowski, E. J.; Felthouse, T. R.; Hendrickson, D. N.; Long, G. J. *Inorg. Chem.* **1976**, *15*, 2908.

(10) Figgis, B. N.; Lewis, J. In "Modern Coordination Chemistry"; Lewis, J., Wilkins, R. G., Eds.; Interscience: New York, 1960; p 403.

(11) Chandler, J. P. Program 66, Quantum Chemistry Program Exchange; Indiana University: Bloomington, Ind.

Mössbauer data were collected on a previously described instrument.[12]

Crystal Measurements. A deep maroon crystal of $[LFe_2(Im)_4](BF_4)_2$ with dimensions 0.18 × 0.25 × 0.38 mm was used for data collection. Preliminary examination of the crystal and data collection were preformed on a Syntex $P2_1$ four-circle automatic diffractometer equipped with a graphite monochromator. The unit cell parameters, listed in Table I, were obtained by a least-squares fit to the automatically centered settings for 15 reflections.[13] The space group used was $C2/c$. All subsequent refinements were done in this space group. After symmetry-equivalent reflections were averaged, a total of 4717 reflections were obtained; of these 2468 were considered above zero at the $1.5\sigma(I)$ significance level. A calculation of the transmission range (0.82–0.86) indicated that no absorption correction was necessary. There was no evidence for crystal decomposition. Lorentz and polarization corrections were applied, but no corrections were deemed necessary for either absorption or extinction.

Structure Solution and Refinement. The structure was solved by the usual heavy-atom techniques using Patterson and Fourier maps in the space group $C2/c$. The center of the cation is at the inversion center $^1/_4, ^1/_4, ^1/_2$. There is disorder at the methylene bridge of the cation at C(7) and at the BF_4^- anion at B(2). The disorder at the latter is a twofold rotation about the B(2)–F(3) bond. The disorder at C(7) showed up initially as a highly anisotropic ellipsoid at C(7). When the atom C(7) was removed, there were two peaks in the difference maps which were near atom C(7). The heights of these peaks were in the approximate ratio 2:1. Refinement, holding all parameters fixed except the occupancies and positions of the major and minor sites of C(7), converged to $g(C(7))/g(C(7'))$ of 0.70/0.30. In subsequent refinements the positional and anisotropic thermal parameters for all nonhydrogen atoms were allowed to vary. Hydrogen atom positions were calculated according to standard criteria and were not allowed to vary. The hydrogen atoms were assigned a fixed isotropic thermal parameter of 7.0. Final, full-matrix, least-squares refinements converged to agreement factors of $R_1 = 0.082$, $R_2 = 0.083$, and $E = 1.25$, where $R_1 = \sum||F_o| - |F_c||/\sum|F_o|$, $R_2 = \sum w||F_o| - |F_c||^2/\sum w|F_o|^2$ and $E = [\sum w||F_o| - |F_c||^2/(m-n)]^{1/2}$, where m is the number of observations and n is the number of variables. The scattering curves used for Fe^{2+}, O^-, and neutral atoms were taken from the analytical expression used in ref 14. The anomalous dispersion effects for iron were included in the structure factor calculations.[15] A final difference map showed the highest peak (height = 0.72 e/Å^3) on the twofold axis at (0.50, 0.12, 0.25) which is ~1.8 Å from B(1) and 1.5 Å from F(2). The next six peaks are 0.58–0.48 e/Å^3 in height and are within 1 Å of Fe^{2+} and F(2). These residual peaks do not fit any disorder model for the BF_4^- group situated about B(1). The final positional and thermal parameters are given in Tables II and III, respectively.

Results

Compound Synthesis and Characterizataion. The formation of binuclear macrocyclic complexes of Fe^{II}, Co^{II}, and Ni^{II} of the type $[LM_2(py)_4]X_2$ (X = BF_4^- or ClO_4^-) from the condensation of 2,6-diformyl-4-methylphenol and 1,3-diaminopropane proceeds readily in pyridine solution. The isolation of binuclear compounds of these metals with noncoordinating anions is in contrast to the results obtained in other solvents. For example, the principal material recovered from the reaction employing $Ni(ClO_4)_2 \cdot 6H_2O$ in methanol was reported to be a mononuclear complex, $LH_2Ni(ClO_4)_2 \cdot 2H_2O$.[3] When the anion is chloride or bromide, the incorporation of two metal ions occurs in methanol.

The initial concern with these species was to ascertain the coordination geometry about the metal atoms. Previous structure determinations have shown that the macrocycle L is capable of accommodating several metal stereochemistries including square pyramidal, octahedral, and square planar.[4,16] Though it would probably involve severe distortion of the ligand, a tetrahedral arrangement may also be possible. In the absence of structural information the distinction among

Table II. Final Positional Parameters[a] for $[LFe_2(Im)_4](BF_4)_2$ Including Hydrogen Atoms[b]

atom	x	y	z
Fe	0.19877 (5)	0.18140 (6)	0.47625 (8)
O	0.2293 (2)	0.2672 (3)	0.3817 (4)
C(2)	0.2129 (4)	0.2799 (4)	0.2698 (6)
C(3)	0.1636 (3)	0.2326 (4)	0.1875 (6)
C(4)	0.1271 (4)	0.1678 (5)	0.2173 (6)
N(5)	0.1344 (3)	0.1403 (4)	0.3180 (5)
C(6)	0.0949 (5)	0.0710 (6)	0.3254 (8)
C(7)	0.0758 (7)	0.0585 (8)	0.4295 (11)
C(7'')	0.1236 (15)	0.0222 (16)	0.4268 (27)
C(8)	0.1298 (5)	0.0415 (5)	0.5437 (8)
N(9)	0.1797 (3)	0.1032 (4)	0.5926 (5)
C(10)	0.2055 (4)	0.1052 (5)	0.7037 (6)
C(11)	0.2435 (4)	0.3399 (4)	0.2260 (6)
C(12)	0.2269 (4)	0.3516 (5)	0.1054 (7)
C(13)	0.1796 (4)	0.3053 (5)	0.0258 (6)
C(14)	0.1487 (4)	0.2467 (5)	0.0686 (6)
C(15)	0.1637 (5)	0.3187 (6)	−0.1037 (7)
N(16)	0.2746 (3)	0.0992 (4)	0.4522 (5)
C(17)	0.3188 (4)	0.0581 (5)	0.5324 (7)
N(18)	0.3626 (3)	0.0220 (4)	0.4924 (7)
C(19)	0.3452 (4)	0.0382 (5)	0.3787 (9)
C(20)	0.2914 (4)	0.0855 (5)	0.3552 (7)
N(21)	0.1144 (3)	0.2538 (4)	0.4903 (5)
C(22)	0.0910 (4)	0.2574 (5)	0.5778 (6)
N(23)	0.0359 (3)	0.3012 (4)	0.5539 (6)
C(24)	0.0220 (4)	0.3268 (6)	0.4455 (8)
C(25)	0.0692 (5)	0.2973 (5)	0.4057 (7)
B(1)	0.0000 (0)	0.5200 (9)	0.2500 (0)
F(1)	−0.0517 (3)	0.4744 (3)	0.2544 (5)
F(2)	−0.0230 (3)	0.5659 (4)	0.1516 (6)
B(2)	0.0000 (0)	0.1450 (14)	−0.2500 (0)
F(3)	0.0000 (0)	0.2259 (5)	−0.2500 (0)
F(4)	−0.0042 (22)	0.1163 (19)	−0.1545 (44)
F(5)	0.0530 (20)	0.2254 (18)	−0.2638 (44)
F(6)	−0.0563 (36)	0.1324 (18)	−0.3382 (54)
H(4)	0.092 (0)	0.142 (0)	0.151 (0)
H(6A)	0.122 (0)	0.024 (0)	0.317 (0)
H(6B)	0.052 (0)	0.073 (0)	0.258 (0)
H(6A')	0.089 (0)	0.038 (0)	0.255 (0)
H(6B')	0.050 (0)	0.089 (0)	0.326 (0)
H(7A)	0.044 (0)	0.013 (0)	0.413 (0)
H(7B)	0.052 (0)	0.107 (0)	0.441 (0)
H(7A')	0.170 (0)	0.011 (0)	0.428 (0)
H(7B')	0.096 (0)	−0.027 (0)	0.410 (0)
H(8A)	0.155 (0)	−0.006 (0)	0.532 (0)
H(8B)	0.107 (0)	0.030 (0)	0.602 (0)
H(8A')	0.143 (0)	−0.006 (0)	0.592 (0)
H(8B')	0.085 (0)	0.060 (0)	0.546 (0)
H(10)	0.189 (0)	0.064 (0)	0.748 (0)
H(12)	0.250 (0)	0.394 (0)	0.076 (0)
H(14)	0.114 (0)	0.213 (0)	0.012 (0)
H(15A)	0.194 (0)	0.333 (0)	−0.139 (0)
H(15B)	0.128 (0)	0.360 (0)	−0.125 (0)
H(15C)	0.144 (0)	0.268 (0)	−0.141 (0)
H(17)	0.319 (0)	0.054 (0)	0.615 (0)
H(18)	0.401 (0)	−0.011 (0)	0.538 (0)
H(19)	0.368 (0)	0.019 (0)	0.323 (0)
H(20)	0.268 (0)	0.108 (0)	0.277 (0)
H(22)	0.113 (0)	0.230 (0)	0.654 (0)
H(23)	0.009 (0)	0.313 (0)	0.608 (0)
H(24)	−0.016 (0)	0.361 (0)	0.402 (0)
H(25)	0.071 (0)	0.306 (0)	0.326 (0)

[a] Standard deviations of the least significant figures are given in parentheses and are given in this fashion in succeeding tables. [b] The hydrogen atom positions were calculated with fixed bond lengths of 1.0 Å.

(12) Munck, E.; Debrunner, P. G.; Tsibris, J. C. M.; Gunsalvs, I. C. *Biochemistry* **1972**, *11*, 855.
(13) All crystallographic calculations were carried out on the Syntex EXTL X-ray crystallographic package, based on the Data Genereal ECLIPSE computer.
(14) "International Tables for X-ray Crystallography"; Ibers, J. A., Hamilton, W. C., Eds.; Kynoch Press: Birmingham, England, 1974; Vol. IV, pp 99, 102.
(15) Reference 14, pp 148, 150.
(16) Gagné, R. R.; Henling, L. M.; Kistenmacher, T. J. *Inorg. Chem.* **1980**, *19*, 1905.

Table III. Anisotropic Thermal Parameters[a] for $[LFe_2(Im)_4](BF_4)_2$[b]

atom	B_{11}	B_{22}	B_{33}	B_{12}	B_{13}	B_{23}
Fe	0.00176 (3)	0.00303 (4)	0.00415 (7)	−0.00011 (3)	0.00110 (3)	0.00002 (6)
O	0.0023 (1)	0.0030 (2)	0.0027 (3)	−0.0002 (1)	0.0007 (2)	−0.00
C(2)	0.0022 (2)	0.0033 (3)	0.0039 (5)	0.0008 (2)	0.0012 (7)	0.0003 (3)
C(3)	0.0019 (2)	0.0030 (3)	0.0037 (5)	0.0006 (2)	0.0008 (3)	−0.0002 (3)
C(4)	0.0021 (2)	0.0046 (4)	0.0037 (5)	0.0003 (2)	0.0005 (3)	−0.0004 (4)
N(5)	0.0017 (2)	0.0036 (3)	0.0061 (5)	−0.0003 (2)	0.0013 (2)	−0.0005 (3)
C(6)	0.0032 (3)	0.0064 (5)	0.0079 (8)	−0.0018 (3)	0.0014 (4)	−0.0014 (6)
C(7)	0.0030 (4)	0.0043 (6)	0.0072 (11)	−0.0007 (4)	−0.0012 (6)	−0.0006 (7)
C(7″)	0.0027 (9)	0.0026 (12)	0.0116 (33)	−0.0012 (8)	0.0028 (14)	−0.0035 (16)
C(8)	0.0041 (3)	0.0037 (4)	0.0081 (8)	−0.0006 (3)	0.0024 (4)	0.0006 (5)
N(9)	0.0025 (2)	0.0027 (3)	0.0063 (6)	−0.0004 (2)	0.0018 (3)	0.0002 (3)
C(10)	0.0029 (2)	0.0036 (4)	0.0048 (6)	0.0008 (2)	0.0016 (3)	0.0014 (4)
C(11)	0.0023 (2)	0.0030 (3)	0.0043 (5)	0.0002 (2)	0.0011 (3)	−0.0000 (3)
C(12)	0.0035 (3)	0.0036 (3)	0.0053 (7)	0.0011 (3)	0.0017 (4)	0.0014 (4)
C(13)	0.0033 (3)	0.0046 (4)	0.0035 (5)	0.0013 (3)	0.0013 (3)	0.0002 (4)
C(14)	0.0025 (2)	0.0045 (4)	0.0053 (6)	0.0007 (3)	0.0012 (3)	−0.0003 (4)
C(15)	0.0049 (4)	0.0065 (5)	0.0046 (6)	0.0013 (4)	0.0019 (4)	0.0014 (4)
N(16)	0.0020 (2)	0.0039 (3)	0.0061 (6)	0.0001 (2)	0.0012 (3)	0.0004 (3)
C(17)	0.0026 (3)	0.0045 (4)	0.0078 (8)	0.0001 (3)	0.0013 (4)	−0.0001 (5)
N(18)	0.0026 (2)	0.0042 (4)	0.0104 (8)	0.0009 (2)	0.0012 (3)	−0.0017 (4)
C(19)	0.0028 (3)	0.0042 (4)	0.0116 (10)	−0.0000 (3)	0.0032 (4)	−0.0017 (5)
C(20)	0.0032 (3)	0.0042 (4)	0.0072 (7)	0.0002 (3)	0.0027 (4)	−0.0002 (4)
N(21)	0.0022 (2)	0.0035 (3)	0.0048 (5)	−0.0000 (2)	0.0014 (2)	−0.0000 (3)
C(22)	0.0030 (3)	0.0039 (4)	0.0055 (6)	0.0006 (3)	0.0016 (3)	−0.0002 (4)
N(23)	0.0028 (2)	0.0043 (4)	0.0100 (7)	0.0005 (2)	0.0028 (3)	−0.0002 (4)
C(24)	0.0032 (3)	0.0042 (4)	0.0110 (9)	0.0014 (3)	0.0021 (4)	0.0020 (5)
C(25)	0.0034 (3)	0.0044 (4)	0.0068 (7)	0.0012 (3)	0.0018 (4)	0.0007 (4)
B(1)	0.0022 (4)	0.0039 (7)	0.0127 (17)	0.0000 (0)	0.0026 (7)	0.0000 (0)
F(1)	0.0034 (2)	0.0068 (3)	0.0132 (6)	−0.0008 (2)	0.0033 (3)	−0.0004 (3)
F(2)	0.0044 (2)	0.0074 (3)	0.0216 (9)	−0.0011 (2)	0.0009 (4)	0.0066 (5)
B(2)	0.0066 (12)	0.0051 (11)	0.0127 (23)	0.0000 (0)	0.0042 (14)	0.0000 (0)
F(3)	0.0076 (4)	0.0041 (4)	0.0171 (11)	0.0000 (0)	0.0078 (6)	0.0000 (0)
F(4)	0.0095 (13)	0.0088 (15)	0.0441 (56)	0.0052 (13)	0.0173 (26)	0.0141 (27)
F(5)	0.0083 (11)	0.0060 (12)	0.0490 (68)	0.0039 (11)	0.0178 (28)	0.0063 (23)
F(6)	0.0181 (27)	0.0094 (14)	0.0487 (69)	−0.0007 (20)	−0.0157 (37)	0.0060 (32)

[a] The form of the anisotropic thermal ellipsoids is given by $\exp[(-B_{11}h^2 + B_{22}k^2 + B_{33}hk + 2B_{13}hl + 2B_{23}kl)]$. All hydrogen atoms were assigned the same isotropic thermal parameters. [b] $B = 7$ (0) Å^2 for all hydrogen atoms.

Table IV. Faraday Magnetic Moments

compd	μ_{eff}/M^{2+} (298 K), μ_B	compd	μ_{eff}/M^{2+} (298 K), μ_B
$[LCo_2(py)_4](BF_4)_2$	4.84 ± 0.05	$[LNi_2(py)_4](ClO_4)_2$	2.87
		$[LFe_2(py)_{3.5}](BF_4)_2$	4.81
$[LCo_2(py)_4](ClO_4)_2$	4.88	$[LFe_2(MeIm)_4](BF_4)_2$	4.71
$[LNi_2(py)_4](BF_4)_2$	2.88	$[LFe_2(MeNic)_4](BF_4)_2$	5.16

ligand geometries must be based on the interpretation of available spectral and magnetic data.

Certain mononuclear complexes of Co^{II} and Ni^{II} with Schiff bases and β-ketoenolates when dissolved in pyridine manifest changes in spectral and magnetic behavior consistent with the formation of octahedral and occasionally five-coordinate species. In several cases bis(pyridine) complexes have been isolated and a few characterized crystallographically. More recently pyridine adducts of binuclear Co^{II} and Ni^{II} complexes of the 1,5-diphenyl-1,3,5-pentanetrionato anion were prepared and their octahedral geometries confirmed by structure determinations.[17,18]

The infrared spectra of the four Co^{II} and Ni^{II} complexes are virtually indistinguishable, the only difference being the positions of the bands due to BF_4^- and ClO_4^-; e.g., $\nu_3(T_2)$ occurs at 1050 cm^{-1} for BF_4^- and at 1090 cm^{-1} for ClO_4^-. All other bands are attributable to L or py.[3] It appears likely that these materials are isostructural in the solid state.

Table V. Electronic Absorption Spectra

compd	medium[a]	$\bar{\nu}$, cm^{-1} [b]
$[LCo_2(py)_4](BF_4)_2$	solid	19.4 sh, 18.4 sh, 10.3
	CH_3CN	10.4 (20), 8.3 sh
	DMF	10.4 (15), 8.3 sh
$[LCo_2(py)_4](ClO_4)_2$	solid	19.4 sh, 18.4 sh, 10.3
	CH_3CH	10.4, 8.3 sh
$[LNi_2(py)_4](BF_4)_2$	solid	21.7 sh, 18.2, 12.1, 10.2
	CH_3CN	17.7, 12.4, 10.1
	DMF	17.7, 12.6, 9.4
$[LNi_2(py)_4](ClO_4)_2$	solid	21.5 sh, 18.2, 12.5, 10.0
	CH_3CN	17.7 (30), 12.4 (5), 10.2 (15)
	DMF	17.7, 12.6, 94
$[LFe_2(py)_4](BF_4)_2$	solid	19.8, 11.1
	pyridine	30.0 (8000), 2.22 (3100), 19.8 (3100), 11.0 (24)
$[LFe_2(MeIm)_4](BF_4)_2$	solid	18.0
	MeIM	30.0 (8000), 22.2 (1800), 18.0 (1800)
$[LFe_2(MeNic)_4](BF_4)_2$	solid	20.0
	MeNic	30.0 (8000), 27.0 (2400), 22.2 (2400), 11.3 (17)

[a] Solid spectra recorded as Nujol mulls. [b] Extinction coefficient given in parentheses (M^{-1} cm^{-1}).

The magnetic and electronic spectral properties of Co^{II} and Ni^{II} are often diagnostic of metal stereochemistry. The Faraday magnetic moments (Table IV) indicate that the complexes are all high spin which is confirmed by the variable-temperature results (vide infra). This effectively eliminates a square-planar arrangement for either metal since Co^{II} species

(17) Kuszaj, J. M.; Tomlonovic, B.; Lintvedt, R. L.; Glick, M. D. *Inorg. Chem.* **1973**, *12*, 1297.
(18) Lintvedt, R. L.; Borer, L. L.; Murtha, D. P.; Kuszaj, J. M.; Glick, M. D. *Inorg. Chem.* **1974**, *13*, 18.

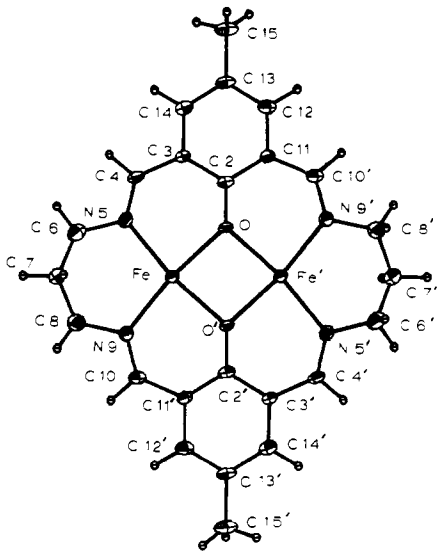

Figure 1. ORTEP plot of the ligand L and coordinated ferrous ions.

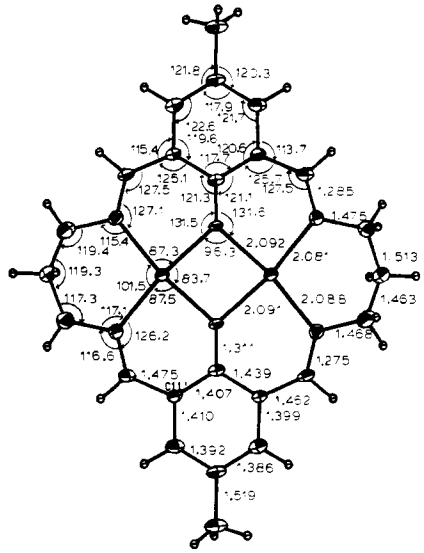

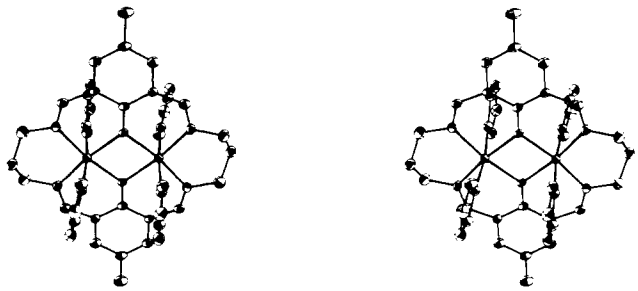

Figure 2. Stereoscopic view of the cation $[LFe_2(Im)_4]^{2+}$.

are invariably low spin and those of Ni^{II} are diamagnetic. The magnetic moments for both complexes lie within their usual ranges for octahedral geometries. However, these values are also consistent with five-coordinate structures.

Electronic spectra were recorded for both solution and solid phases (Table V). High-intensity absorptions of intraligand and/or charge-transfer origin which occur in the UV region may obscure higher energy ligand field bands. Indeed shoulders are observed on these bands in solid-state spectra. The spectra are qualitatively similar in all media although there is some variation in the location of band maxima particularly with the nickel materials.

For the cobalt complexes the spectra closely resemble previously reported results for bis(pyridine) adducts of mononuclear species in the appropriate N_2O_2 and O_4 environments and are consistent with octahedral coordination.[19] Only one well-defined absorption is observed at 10.4×10^3 cm^{-1} although in solution there appears to be a weak feature at 8.3×10^3 cm^{-1} which causes the tail of the former band to fall off less rapidly. The square pyramidal geometry would be expected to give rise to several bands in the near IR region. Moreover the low intensity of this band seems to preclude a tetrahedral structure. In idealized octahedral symmetry the 10.4×10^3 cm^{-1} band would probably correspond to $^4T_{1g}(F) \rightarrow {}^4T_{2g}$, and transitions to higher exicted states (including spin-forbidden processes) occur as the observed shoulders or are obscured by the high-intensity bands.

On the basis of similar comparison of the spectra of $[LNi_2(py)_4]X_2$ species with those of well-established pyridine adducts of analogous mononuclear Ni^{II} complexes, octahedral geometry again appears most reasonable.[19] The position of the lowest energy band is dependent on the medium which may reflect replacement of pyridine by solvent molecules. For the square-pyramidal environment several bands are again anticipated in the near IR at lower frequency than is usually found with octahedral structures. Indeed the spectrum of $LNi_2Cl_2 \cdot 2H_2O$ displays five bands in solution and in the solid state and is believed to be five-coordinate.[3] By analogy with the cobalt system the low intensities of the observed bands also militate against tetrahedral geometry. According to an octahedral model a tentative assignment of the lowest energy band is $^3A_{1g} \rightarrow {}^3T_{2g}$. The next band of increasing energy is quite weak and could arise from a spin-forbidden transition such as $^3A_{1g} \rightarrow {}^1E_g$ which is occasionally observed in Ni^{II} spectra. The 17.7×10^3 cm^{-1} band is then due to $^3Ag_{1g} \rightarrow {}^3T_{1g}(F)$, and the shoulder at $\sim 21.7 \times 10^3$ cm^{-1} is attributable to $^3A_{1g} \rightarrow {}^3T_{1g}(P)$.

The spectra of the high-spin Fe^{II} complexes are dominated by charge-transfer bonds. Significant by its absence is the low-energy d–d band observed in the square-pyramidal Fe_2LCl_2 species at 7.9×10^3 cm^{-1}. It is also noteworthy that little differences exist in comparing solution and solid-state spectra. Weak features at 11.1×10^3 cm^{-1} in the pyridine adducts are tentatively assigned to $^5T_{2g} \rightarrow {}^5E_g$. The corresponding $Fe(H_2O)_6^{2+}$ complex shows this transition at 10.0×10^3 cm^{-1}, consistent with the weaker field aquo ion.[20]

Molecular Structure of $[LFe_2(Im)_4](BF_4)_2$. The single-crystal X-ray structure of this compound was solved by using standard heavy-atom techniques. The structure consists of discrete binuclear $[LFe_2(Im)_4]^{2+}$ cations and BF_4^- anions. Bond distances and angles are given in Table VI and are also indicated in Figure 1. The binuclear cation is located about a crystallographic center of inversion. Each iron ion is coordinated to four atoms of the ligand L as well as two axial imidazole ligands. Least-squares fit planes were calculated for the cation, and, as can be seen by the results given in Table VII, the ligand L in $[LFe_2(Im)_4](BF_4)_2$ is planar except for the disorder at the C(7) carbon atom of the trimethylene bridge. The stereoscopic view of $LFe_2(Im)_4^{2+}$ given in Figure 2 illustrates the planarity of L. Disorder in the trimethylene bridge of the L ligand was also noted for the two five-coordinate complexes.[4,5] This disorder at C(7) is, of course, merely the reflection of two possible sites for the C(7) atom. There

(19) (a) Yamada, S. *Coord. Chem. Rev.* **1966**, *1*, 415. (b) Holm, R. H.; Everett, G. W.; Chakravorty, A. *Prog. Inorg. Chem.* **1966**, *7*, 83.

(20) Dunn, T. M. In "Modern Coordination Chemistry"; Lewis, J., Wilkins, R. G., Eds.; Interscience: New York, 1960; p 290.

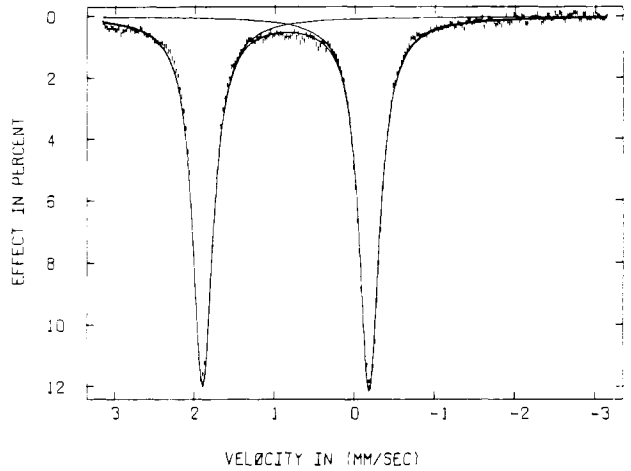

Figure 3. Room-temperature ^{57}Fe Mössbauer spectrum of $[LFe_2(Im)_4](BF_4)_2$.

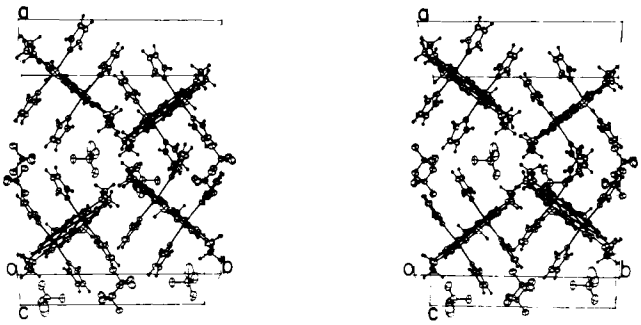

Figure 4. Stereoscopic view of the unit cell for $[LFe_2(Im)_4](BF_4)_2$.

is a decided preference for the C(7) site over the C(7″) site apparently due to steric interactions between atom C(7″) and the array B(2)–F(4).

Of primary importance to the present study of magnetic exchange interactions is the finding that the two iron ions are only 0.011 (1) Å out of the plane of the ligand L. By way of comparison it is to be noted that the metal ions in the five-coordinate complexes of L are considerably removed from the ligand plane. The copper(II) ion is 0.21 Å out of the ligand plane in $LCu_2Cl_2 \cdot 6H_2O$,[4] whereas the high-spin cobalt(II) ion is 0.298 Å out of the ligand plane in $LCo_2Br_2 \cdot CH_3OH$.[5]

The $LFe_2(Im)_4^{2+}$ cation possesses two high-spin iron(II) ions with an Fe–Fe distance of 3.117 (2) Å. The overall charge on the cation, Mössbauer effect data, and magnetic susceptibility data (vide infra) clearly indicate high-spin iron(II) ions. The 4.2 K ^{57}Fe Mössbauer spectrum obtained for the sample of $[LFe_2(Im)_4](BF_4)_2$ used for the crystal structure is shown in Figure 3. There is only one quadrupole-split doublet; least-squares fitting gives a quadrupole splitting of ΔE_Q = 2.0797 (14) mm/s and an isomer shift of δ = 0.7387 (7) mm/s vs. iron metal. Values of ΔE_Q for six-coordinate, high-spin iron(II) complexes have been found to be in the range of 2.0–3.0 mm/s.[21] There is no evidence in the spectrum for the presence of iron(III) in the sample. The room-temperature Mössbauer spectrum for $[LFe_2(MeIm)_4](BF_4)_2$ also shows only one doublet with ΔE_Q = 2.22 (2) mm/s and δ = 0.94 (2) mm/s. In contrast, the high-spin iron(II) ions in LFe_2Cl_2 give a Mössbauer spectrum (ambient temperature) consisting of one doublet with an appreciably larger quadrupole splitting: ΔE_Q = 3.600 (10) mm/s and δ = 0.941 (5) mm/s.

Figure 4 gives a stereoscopic view of the unit cell for $[LFe_2(Im)_4](BF_4)_2$, where it can be seen that the binuclear

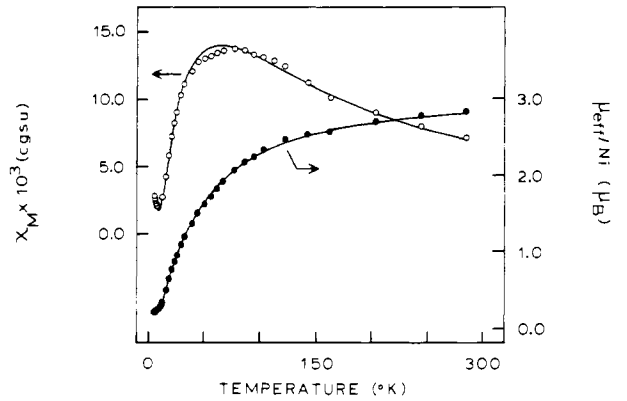

Figure 5. Molar paramagnetic susceptibility χ_M, and effective magnetic moment, μ_{eff}/Ni, vs. temperature curves for $[LNi_2(py)_4](BF_4)_2$. The solid lines represent the least-squares fit of the data to the theoretical equation given in the text.

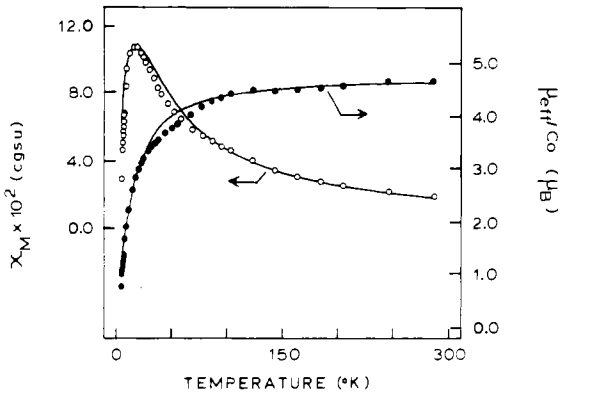

Figure 6. Molar paramagnetic susceptibility, χ_M, and effective magnetic moment, μ_{eff}/Co, vs. temperature curves for $[LCo_2(py)_4](BF_4)_2$. The solid lines represent the least-squares fit of the data to the theoretical equation given in the text.

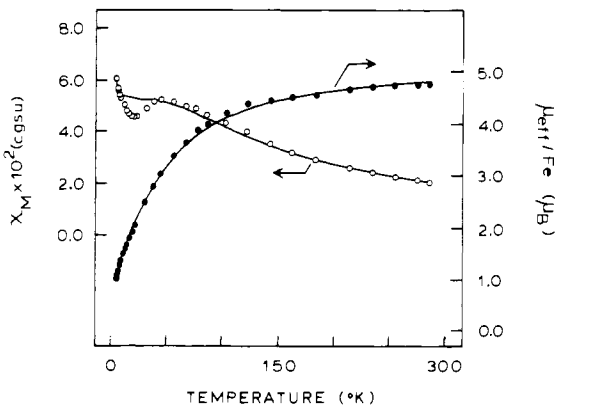

Figure 7. Molar paramagnetic susceptibility, χ_M, and effective magnetic moment, μ_{eff}/Fe, vs. temperature curves for $[LFe_2(py)_4](BF_4)_2$. The solid lines represent the least-squares fit of the data to the theoretical equation given in the text.

cations are reasonably well isolated from each other. Not shown is the disorder present in the BF_4^- ion, which consists of a twofold rotation about B(2)–F(3) and appears only at B(2). There are no strong intermolecular hydrogen bonds. The range of normal hydrogen bonds of the type N–H···F is 2.61–2.82 Å,[22] and it can be seen in Table VIII[22] that one of the intermolecular contacts in $[LFe_2(Im)_4](BF_4)_2$ is within this range.

(21) Merrill, P. H.; Goedken, V. I.; Busch, D. H.; Stone, J. A. *J. Am. Chem. Soc.* **1975**, *92*, 7590.

(22) Supplementary material.

Table VI. Principal Interatomic Distances (Å) and Angles (Deg) for $[LFe_2(Im)_4](BF_4)_2$

Distances within $[LFe_2(Im)_4]^{2+}$			
Fe-N(16)	2.218 (7)	N(9)-C(10)	1.285 (10)
Fe-N(21)	2.218 (7)	C(10)-C(11)	1.475 (11)
Fe-O′	2.091 (4)	C(11)-C(12)	1.410 (10)
Fe-O	2.092 (5)	C(12)-C(13)	1.392 (12)
Fe-N(5)	2.088 (6)	C(13)-C(14)	1.386 (12)
Fe-N(9)	2.081 (6)	C(13)-C(15)	1.519 (10)
O′-C(2)	1.311 (8)	C(14)-C(3)	1.399 (10)
C(2)-C(3)	1.439 (10)	N(16)-C(17)	1.317 (11)
C(2)-C(11)	1.407 (11)	C(17)-N(18)	1.326 (12)
C(3)-C(4)	1.462 (11)	N(18)-C(19)	1.341 (13)
C(4)-N(5)	1.275 (9)	C(19)-C(20)	1.347 (13)
N(5)-C(6)	1.468 (12)	C(20)-N(16)	1.358 (11)
C(6)-C(7)	1.463 (16)	N(21)-C(22)	1.312 (10)
C(6)-C(7″)	1.451 (31)	C(22)-N(23)	1.333 (12)
C(7)-C(8)	1.513 (16)	N(23)-C(24)	1.329 (12)
C(7″)-C(8)	1.426 (32)	C(24)-C(25)	1.339 (14)
C(8)-N(9)	1.475 (11)	C(25)-N(21)	1.374 (11)
Angles within $[LFe_2(Im)_4]^{2+}$			
N(5)-Fe-N(16)	86.8 (2)	O′-Fe-N(21)	92.6 (2)
O-Fe-N(21)	94.9 (2)	O′-Fe-N(16)	90.7 (2)
O-Fe-N(16)	92.9 (2)	O′-Fe-O	83.7 (2)
O-Fe-N(5)	87.3 (2)	C(2)-C(11)-C(12)	120.6 (7)
O-Fe-N(9)	171.2 (2)	C(11)-C(12)-C(13)	121.7 (8)
O′-Fe-N(5)	171.0 (2)	C(12)-C(13)-C(14)	117.9 (8)
O′-Fe-N(9)	87.5 (2)	C(12)-C(13)-C(15)	120.3 (8)
N(5)-Fe-N(9)	101.5 (3)	C(14)-C(13)-C(15)	121.8 (8)
Fe-O-Fe′	96.3 (2)	C(13)-C(14)-C(3)	122.6 (8)
C(2)-O-Fe	131.6 (5)	C(20)-N(16)-C(17)	103.4 (7)
C(2)-O-Fe	131.5 (5)	N(16)-C(17)-N(18)	112.7 (8)
O-C(2)-C(3)	121.3 (7)	C(17)-N(18)-C(19)	107.0 (8)
O-C(2)-C(11)	121.1 (7)	N(18)-C(19)-C(20)	106.0 (8)
C(3)-C(2)-C(11)	117.7 (7)	C(19)-C(20)-N(16)	110.9 (8)
C(2)-C(3)-C(14)	119.6 (7)	C(25)-N(21)-C(22)	103.4 (7)
C(2)-C(3)-C(4)	125.1 (7)	N(21)-C(22)-N(23)	112.2 (7)
C(4)-C(3)-C(14)	115.4 (7)	C(22)-N(23)-C(24)	107.4 (8)
C(3)-C(4)-N(5)	127.5 (7)	C(24)-C(25)-N(21)	110.4 (8)
C(4)-N(5)-Fe	127.1 (5)	Fe-N(16)-C(17)	127.5 (6)
C(16)-N(5)-Fe	115.4 (5)	Fe-N(16)-C(20)	128.7 (5)
C(4)-N(5)-C(16)	117.5 (7)	Fe-N(21)-C(22)	127.5 (3)
N(5)-C(6)-C(7)	119.4 (9)	Fe-N(21)-C(25)	128.6 (5)
N(5)-C(6)-C(7″)	115.4 (14)	N(5)-Fe-N(21)	87.8 (2)
C(6)-C(7)-C(8)	119.3 (10)	N(9)-Fe-N(21)	89.2 (2)
C(6)-C(7″)-C(8)	126 (2)	N(9)-Fe-N(21)	88.4 (2)
C(7)-C(8)-N(9)	117.3 (8)	N(16)-Fe-N(21)	173.6 (2)
C(7″)-C(18)-N(9)	113.1 (4)		
C(10)-N(9)-Fe	117.1 (5)	C(10)-N(9)-Fe	126.2 (5)
C(8)-N(9)-C(10)	116.6 (7)	N(9)-C(10)-C(11)	127.5 (7)
C(10)-C(11)-C(12)	113.7 (7)	C(10)-C(11)-C(2)	125.7 (7)
Distances within the Tetrafluoroborate Anion			
B(1)-F(1)	1.355 (11)	B(1)-F(2)	1.382 (12)
B(2)-F(3)	1.39 (3)	B(2)-F(4)	1.29 (5)
B(2)-F(5)	1.29 (4)	B(2)-F(6)	1.34 (7)
Angles within the Tetrafluoroborate Anion			
F(1)-B(1)-F(1′)	109.5 (7)	F(4′)-B(2)-F(6′)	111 (3)
F(1)-B(1)-F(2)	107.5 (7)	F(5)-B(2)-F(6)	114 (3)
F(1)-B(1)-F(2′)	110.8 (8)	F(5′)-B(2)-F(6′)	114 (3)
F(2)-B(1)-F(2′)	110.8 (7)	F(4)-B(2)-F(4′)	135 (3)
F(3)-B(2)-F(4)	112 (2)	F(5)-B(2)-F(5′)	133 (3)
F(3)-B(2)-F(4′)	112 (2)	F(6)-B(2)-F(6′)	161 (4)
F(3)-B(2)-F(5)	113 (2)	F(4)-B(2)-F(5′)	54 (3)
F(3)-B(2)-F(5′)	113 (2)	F(4′)-B(2)-F(5)	54 (3)
F(3)-B(2)-F(6)	99 (3)	F(4)-B(2)-F(6′)	61 (3)
F(3)-B(2)-F(6′)	99 (3)	F(4′)-B(2)-F(6)	61 (3)
F(4)-B(2)-F(5)	106 (3)	F(5)-B(2)-F(6′)	57 (3)
F(4′)-B(2)-F(5′)	106 (3)	F(5′)-B(2)-F(6)	57 (3)
F(4)-B(2)-F(6)	111 (3)		

Magnetic Susceptibility. Variable-temperature (4.2–285 K) magnetic susceptibility data were collected for $[LFe_2(py)_4](BF_4)_2$, $[LFe_2(MeIm)_4](BF_4)_2$, $[LFe_2(Im)_4](BF_4)_2$, $[LFe_2(MeNic)_4](BF_4)_2$, $[LCo_2(py)_4](BF_4)_2$, and $[LNi_2(py)_4](BF_4)_2$. The data are given in Tables IX–XIV[22] and are illustrated in Figures 5–9.

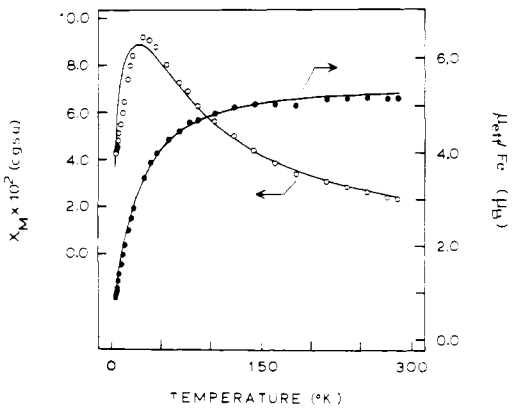

Figure 8. Molar paramagnetic susceptibility, χ_M, and effective magnetic moment, μ_{eff}/Fe, vs. temperature curves for $[LFe_2(MeIm)_4](BF_4)_2$. The solid lines represent the least-squares fit of the data to the theoretical equation given in the text.

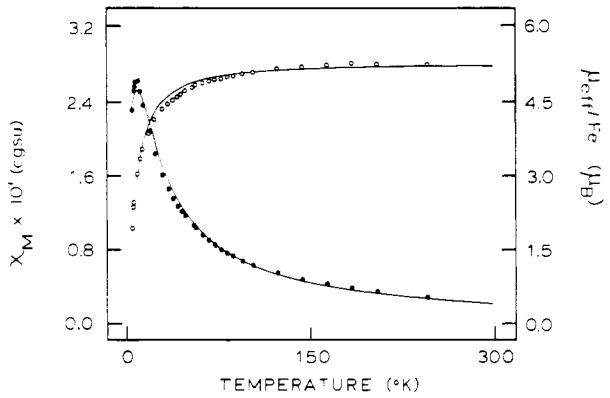

Figure 9. Molar paramagnetic susceptibility, χ_M, and effective magnetic moment, μ_{eff}/Fe, vs. temperature curves for $[LFe_2(Im)_4](BF_4)_2$. The solid lines represent the least-squares fit of the data to the theoretical equation given in the text.

There is a maximum at ca. 70 K in the χ vs. T curve for $[LNi_2(py)_4](BF_4)_2$ (see Figure 5). The effective magnetic moment per nickel ion, μ_{eff}/Ni, varies from 2.83 μ_B at 285 K to 0.21 μ_B at 4.2 K. An antiferromagnetic exchange interaction is present. In order to compare the interactions present in these six-coordinate complexes with those reported[6] for the analogous five-coordinate complexes, it was decided to fit the data to theoretical susceptibility expressions that result from the spin Hamiltonian for an isotropic magnetic exchange, $\hat{H} = -2J\hat{S}_1\cdot\hat{S}_2$. In the case of a binuclear nickel(II) complex, $S_1 = S_2 = 1$ and the molar paramagnetic susceptibility for the binuclear complex is given by eq 1, where the symbols have

$$\chi_M = \frac{Ng^2\beta^2}{kT}\left[\frac{10 + 2\exp(-4J/kT)}{5 + 3\exp(-4J/kT) + \exp(-6J/kT)}\right] \quad (1)$$

the usual meanings. Least-squares fitting the data for $[LNi_2(py)_4](BF_4)_2$ to eq 1 gives $J = -23$ cm^{-1} and $g = 2.13$. As can be seen in Figure 5, the fit (solid lines) is good.

The compound $[LCo_2(py)_4](BF_4)_2$ also exhibits a χ vs. T curve with a maximum, in this case at ca. 16 K (see Figure 6). The values of μ_{eff}/Co vary from 4.55 μ_B at 285 K to 0.69 μ_B at 4.2 K. Each cobalt(II) ion is high spin. The molar paramagnetic susceptibility for an $S_1 = S_2 = {}^3/_2$ binuclear complex is given by eq 2. Fitting the data to this equation

$$\chi_M = \frac{Ng^2\beta^2}{kT}[28 + 10\exp(-6J/kT) + 2\exp(-10J/kT)]/[7 + 5\exp(-6J/kT) + 3\exp(-10J/kT) + \exp(-12J/kT)] \quad (2)$$

Table VII

Least-Squares Planes for $[LFe_2(Im)_4](BF_4)_2$

atom	dist, Å	atom	dist, Å
	Ligand Plane,[a] Plane 1, $\chi^2 = 4979$		
O	−0.065 (5)	C(8)	0.098 (10)
	[0.065 (5)][b]		[−0.098 (10)]
C(2)	−0.035 (8)	N(9)	0.064 (6)
	[0.035 (8)]		[−0.064 (6)]
C(3)	−0.017 (7)	C(10)	0.035 (9)
	[0.017 (7)]		[−0.035 (9)]
C(4)	−0.035 (8)	C(11)	−0.009 (8)
	[0.035 (8)]		[0.009 (8)]
N(5)	−0.010 (6)	C(12)	0.061 (9)
	[0.010 (6)]		[−0.061 (9)]
C(6)	0.056 (10)	C(13)	0.092 (9)
	[−0.056 (10)]		[−0.092 (9)]
C(7)	−0.525 (14)	C(14)	0.049 (9)
	[0.525 (14)]		[−0.0.49 (9)]
C(7″)	0.656 (31)		
	[−0.656 (31)]		
	Imidazole "A" Plane, Plane 2, $\chi^2 = 8.62$		
N(16)	−0.005 (7)	C(19)	0.004 (9)
C(17)	0.013 (9)	C(20)	0.004 (9)
N(18)	−0.007 (8)		
	Imidazole "B" Plane, Plane 3, $\chi^2 = 2.94$		
N(21)	−0.005 (6)	C(24)	−0.005 (10)
C(22)	0.007 (8)	C(25)	0.010 (9)
N(23)	−0.002 (7)		
	Ligand Plane,[c] Plane 4, $\chi^2 = 1652$		
O	−0.072 (5)	N(9)	0.046 (6)
	[0.072 (5)][b]		[−0.046 (6)]
C(2)	−0.049 (8)	C(10)	0.026 (9)
	[0.049 (8)]		[−0.026 (9)]
C(3)	−0.046 (7)	C(11)	−0.015 (8)
	[0.046 (7)]		[0.015 (8)]
C(4)	−0.074 (8)	C(12)	0.047 (9)
	[0.074 (8)]		[−0.047 (9)]
N(5)	−0.045 (6)	C(13)	0.064 (9)
	[0.045 (6)]		[−0.064 (9)]
C(6)	0.010 (10)	C(14)	0.013 (9)
	[−0.010 (10)]		[−0.013 (9)]
C(8)	0.064 (10)	C(15)	0.155 (11)
	[−0.064 (10)]		[−0.155 (11)]
	Benzene Ring Plane, Plane 5, $\chi^2 = 1.75$		
C(2)	0.007 (8)	C(12)	0.000 (9)
C(3)	−0.003 (7)	C(13)	0.004 (9)
C(1)	−0.005 (8)	C(14)	−0.002 (9)

Angles between Planes

plane	plane	angle, deg	plane	plane	angle, deg
1	2	85.8	2	4	86.3
1	3	80.7	2	5	85.6
1	4	0.6	3	4	81.3
1	5	2.6	3	5	80.9
2	3	8.7	4	5	2.5

[a] The ferrous ions are located 0.011 (1) Å out of this plane. [b] The values in brackets denote the out-of-plane distance for those atoms related to the listed atom by inversion. [c] The ferrous ions are located 0.026 (1) Å out of this plane.

gives the solid lines in Figure 2, which are characterized by $J = -4.1$ cm^{-1} and $g = 2.41$.

The axial ligands for two of the iron(II) compounds are pyridines. Figure 7 shows the data for $[LFe_2(py)_4](BF_4)_2$. The data obtained for $[LFe_2(MeNic)_4](BF_4)_2$ are very similar in appearance. As can be seen in Figure 7, there is an increase in χ_M at low temperatures following the maximum at ca. 44 K. This increase in χ_M at temperatures less than ca. 17 K is most likely attributable to a small amount of a paramagnetic impurity. The impurity could, for instance, be either a binucleating ligand L with only one Fe^{II} or Fe^{III} ion coordinated or some other ferric-containing impurity. The susceptibility

Table XV. Magnetic Exchange Parameters

compd type[a]	J, cm^{-1} Mn^{2+}	Fe^{2+}	Co^{2+}	Ni^{2+}	Cu^{2+}
$LM_2Cl_2 \cdot nH_2O$[b] (five coordinate)	+0.20	−4.2	−6.0	−27	−294
$[LM_2(py)_4](BF_4)_2$		−7.5	−4.1	−23	
$[LM_2(MeNic)_4](BF_4)_2$		−6.8			
$[LM_2(MeIm)_4](BF_4)_2$		−4.5			
$[LM_2(Im)_4](BF_4)_2$		−1.5			

[a] L is the binucleating ligand formed from the condensation of 2 mol of 2,6-diformyl-4-methylphenol with 2 mol of 1,3-diaminopropane. [b] All of these data, except the J value for the Co–Cl case, are from ref 6. The J value for $LCo_2Cl_2 \cdot 2CH_3OH$ was determined in this study.

equation for an $S_1 = S_2 = 2$ binuclear complex can be easily derived. A second term accounting for the paramagnetic impurity was added to this equation to give eq 3. In eq 3,

$$\chi_M = \frac{Ng^2\beta^2}{kT}[60 + 28\exp(-8J/kT) + 10\exp(-14J/kT) + 2\exp(-18J/kT)]/[9 + 7\exp(-8J/kT) + 5\exp(-14J/kT) + 3\exp(-18J/kT) + \exp(-20J/kT)] + \frac{4.2(\mathrm{PARA})}{T} \quad (3)$$

PARA is the molar paramagnetic susceptibility of the impurity at 4.2 K.

Least-squares fitting the data for $[LFe_2(py)_4](BF_4)_2$ to eq 3 gives $J = -7.5$ cm^{-1}, $g = 2.10$, and PARA = 0.0564 cgsu. The value of PARA corresponds to ca. 6% by weight of $[LFe(py)_2]BF_4$. Fitting the data for $[LFe_2(MeNic)_4](BF_4)_2$ gave $J = -6.8$ cm^{-1}, $g = 1.98$, and PARA = 0.0581 cgsu, where the PARA value corresponds to ca. 7% by weight of $[LFe(MeNic)_2]BF_4$. There is no evidence of paramagnetic impurity in the susceptibility data for $[LFe_2(MeIm)_4](BF_4)_2$, as can be seen in Figure 8. Fitting the data for this compound to eq 3 with PARA fixed at zero gave $J = -4.5$ cm^{-1} and $g = 2.25$. The magnetic susceptibility data for $[LFe_2(Im)_4](BF_4)_2$ are illustrated in Figure 9. In this case the best fitting parameters were found to be $J = -1.5$ cm^{-1} and $g = 2.17$.

Discussion

The magnetic exchange parameters for the six-coordinate $[LM_2(base)_4](BF_4)_2$ complexes studied in this paper are summarized in Table XV together with the J values reported[6] previously for the analogous five-coordinate complexes. The variation in magnetic exchange parameter across the series of five-coordinate LM_2Cl_2 complexes was attributed to two factors. The structural work on $LCo_2Br_2 \cdot CH_3OH$[4] and $Cu_2Cl_2 \cdot 6H_2O$[5] demonstrates the variation in metal–ligand plane distance. The second important factor that varies across the series is the number (and spatial distribution) of unpaired electrons.

Because the ligand L is expected to be relatively rigid, the first of these factors could be eliminated, or at least minimized, by constraining the metal ions to lie in the plane of the ligand L. This was accomplished by preparing six-coordinate complexes of the binucleating ligand L. In the Results it was shown via electronic absorption spectroscopy that the nickel(II) and cobalt(II) complexes with composition $[LM_2(py)_4](BF_4)_2$ have six-coordinate metal ions. The X-ray crystal structure of $[LFe_2(Im)_4](BF_4)_2$ confirms six-coordination for iron. With the metal ion constrained to lie in the plane of the ligand L the variation in geometry as the metal ion radius changes should be minimized. It should be possible then to study the effect of the variation of the number and distribution of un-

paired electrons on the magnetic exchange interaction.

Examination of Table XV shows that there are only relatively small differences in J values between the five-coordinate and six-coordinate complexes of a given metal ion. This could result from two opposing factors. When the metal ion is moved into the plane, overlap between the metal-based $d_{x^2-y^2}$ orbitals and the oxygen-based sp^2 hybrid orbitals is increased. Since this σ framework represents the dominant pathway for the superexchange mechanism, the enhanced overlap should result in an *increase* in the antiferromagnetic interaction. On the other hand, these structural changes will result in a stronger ligand field about the metal ions, leading to an enhanced difference between the energies of the metal-based and bridging oxygen atom orbitals. This will decrease the exchange interaction. As is evident from the data, these two effects apparently cancel.

The magnetic susceptibility data for the four $[LFe_2(base)_4](BF_4)_2$ complexes substantiate the statement that an increased ligand field splitting would affect the net antiferromagnetic interaction. The two iron(II) complexes with pyridine bases (py and MeNic) as the axial ligands exhibit approximately the same magnitude of interaction, whereas the two iron(II) complexes with the stronger axial bases (Im and MeIm) exhibit the weaker net antiferromagnetic interaction.

In summary, the two offsetting factors of improved orbital overlap and increased ligand field splitting for the six-coordinate complexes lead to only a small difference in the J values between the five- and six-coordinate complexes of a given metal ion. What is of greater significance is that the exchange parameter does vary appreciably across the $[LM_2(py)_4](BF_4)_2$ [M = Fe(II), Co(II), and Ni(II)] series. It is likely that this variation reflects the changing number of unpaired electrons from one complex to another. In this regard it is important to note that an antiferromagnetic exchange interaction has been noted[23] for MnO, FeO, CoO, and NiO, where the Néel temperatures increase regularly from 116 to 523 K in going from MnO to NiO. Each of these compounds has a rock salt structure, and the exchange interaction occurs through linear M–O–M units. Presumably both the M–O distances and the number of unpaired electrons are important. In contrast, Sinn et al.[24] very recently came to a different conclusion. Magnetic susceptibility data were collected for a series of heterobinuclear complexes. It was concluded that the differences in J values could be entriely accounted for by changes in structure differences in the compounds and did *not* depend on the number of unpaired electrons. It is clear that additional work is needed.

Acknowledgment. We are grateful for support from NIH Grant HL 13652 (to D.N.H.) and NSF Grant CHE79-27141 (to R.R.G.). The National Science Foundation is to be thanked for partial funding to purchase the Syntex $P2_1$ diffractometer at the University of Illinois.

Registry No. $[LFe_2(py)_4](BF_4)_2$, 76136-05-5; $[LFe_2(MeIm)_4](BF_4)_2$, 76136-07-7; $[LFe_2(MeNic)_4](BF_4)_2$, 76156-49-5; $[LFe_2(Im)_4](BF_4)_2$, 76136-09-9; $[LCo_2(py)_4](BF_4)_2$, 76136-11-3; $[LCo_2(py)_4](ClO_4)_2$, 76136-12-4; $[LNi(py)_4](BF_4)_2$, 76136-14-6; $[LNi(py)_4](ClO_4)_2$, 76156-50-8; 1,3-diaminopropane, 109-76-2; 2,6-diformyl-4-methylphenol, 7310-95-4; LCo_2Cl_2, 47737-29-1.

Supplementary Material Available: Tables VIII–XIV (nonbonding contacts, calculated and observed magnetic susceptibility data) and listings of observed and calculated structure factors (37 pages). Ordering information is given on any current masthead page.

(23) Nesbet, R. K. *Phys. Rev.* **1960**, *119*, 658.
(24) O'Connor, C. J.; Freyberg, D. P.; Sinn, E. *Inorg. Chem.* **1979**, *18*, 1077.

Contribution from the Departments of Chemistry, University of Nebraska, Lincoln, Nebraska 68588, and University of California, Berkeley, California 94720

Catalytic Hydrogenation of Aromatic Hydrocarbons. 7.[1] Chemistry and Crystal Structure of (η^3-Cyclooctenyl)cobalt(I) Tris(trimethyl phosphite)

M. R. THOMPSON, V. W. DAY,*[2] K. DAVID TAU, and E. L. MUETTERTIES*

Received September 3, 1980

The synthesis, crystal structure, and catalytic chemistry of allylcobalt(I) phosphite complex (η^3-cyclooctenyl)cobalt(I) tris(trimethyl phosphite) is described. A single-crystal X-ray diffraction study established a $P2_1/n$ space group (a = 9.361 (3) Å, b = 15.302 (5) Å, c = 18.164 (4) Å, β = 101.28 (2)°, Z = 4). Structurally, the molecule may be described as a tetragonal pyramid with a phosphite ligand at the axial site and with a basal edge spanned by the η^3-cyclooctenyl ligand. This molecule like the paradigm of this class of molecules, (η^3-allyl)cobalt tris(trimethyl phosphite), is a catalyst precursor for arene hydrogenation. Consistent with earlier observations, the substitution of bulkier phosphites (ethyl and isopropyl) for trimethyl phosphite raised the catalyst activity and lowered the catalyst lifetime.

Introduction

Allylcobalt tris(phosphite) and -(phosphine) complexes comprise a unique class of catalysts for stereoselective hydrogenation of aromatic hydrocarbons.[3,4] For some years, we have searched[5] for suitable crystals of one of these complexes for a crystallographic analysis and have finally succeeded with a special cyclic allyl derivative. Here we describe the synthesis, crystal structure, and catalytic properties of (η^3-cyclooctenyl)cobalt(I) tris(trimethyl phosphite). There is, aside from the catalytic chemistry, a special relevance of this structure to unusual and closely related allyliron structures reported by Harlow and co-workers.[6]

Experimental Section

Reagents and Solvents. All operations with air-sensitive materials were carried out in a Vacuum Atmospheres drybox under an argon atmosphere, in a conventional vacuum system or by using Schlenk techniques. Trimethyl phosphite, triethyl phosphite, and 1,5-cyclooctadiene were purchased from Aldrich Chemical Co. Inc.; triisopropyl phosphite was purchased from Strem Chemicals. Prepurified hydrogen

* To whom correspondence should be addressed: V.W.D., University of Nebraska; E.L.M., University of California.

(1) Paper 6 in this series: Stuhl, L. S.; Rakowski DuBois, M., Hirsekorn, F. J.; Bleeke, J. R.; Stevens, A. E.; Muetterties, E. L. *J. Am. Chem. Soc.* **1978**, *100*, 2405.
(2) Camille and Henry Dreyfus Teacher-Scholar.
(3) Muetterties, E. L.; Bleeke, J. R. *Acc. Chem. Res.* **1979**, *12*, 324.
(4) Bleeke, J. R.; Muetterties, E. L. *J. Am. Chem. Soc.* **1981** *103*, 556.
(5) We would have preferred to study a single crystal of η^3-C_3H_5Co complex, but all attempts yielded crystals that had poor diffraction properties.
(6) Harlow, R. L.; McKinney, R. J.; Ittel, S. D. *J. Am. Chem. Soc.* **1979**, *101*, 7496.

0020-1669/81/1320-1237$01.25/0